JOURNAL OF PROPULSION AND POWER
Vol. 26, No. 2, March–April 2010

Harmonic Balance Analysis of Blade Row Interactions in a Transonic Compressor

Kivanc Ekici*
University of Tennessee, Knoxville, Tennessee 37996
and
Kenneth C. Hall† and Robert E. Kielb‡
Duke University, Durham, North Carolina 27708

DOI: 10.2514/1.43879

In this paper we apply the harmonic balance technique to analyze an inlet guide vane and rotor interaction problem, and compare the computed flow solutions to existing experimental data. The computed results, which compare well with the experimental data, demonstrate that the technique can accurately and efficiently model strongly nonlinear periodic flows, including shock/vane interaction and unsteady shock motion. Using the harmonic balance approach, each blade row is modeled using a computational grid spanning just a single blade passage regardless of the actual blade counts. For each blade row, several subtime level solutions that span a single time period are stored. These subtime level solutions are related to each other through the time derivative term in the Euler (or Navier–Stokes) equations, which is approximated by a pseudo-spectral operator, by complex periodicity conditions along the periodic boundary of each blade row's computational domain, and by the interface boundary conditions between the vane and rotor. Casting the governing equations in harmonic balance form removes the explicit dependence on time. Mathematically, the equations to be solved are similar in form to the steady Euler (or Navier–Stokes) equations with an additional source term proportional to the fundamental frequency of the unsteadiness. Thus, conventional steady-state computational fluid dynamics techniques, including local time stepping and multigrid acceleration, are used to accelerate convergence, resulting in a very efficient unsteady flow solver.

Nomenclature

A_k, B_k	=	kth temporal Fourier coefficients
$\tilde{\boldsymbol{A}}_{lm}$, $\tilde{\boldsymbol{B}}_{lm}$	=	lmth Fourier coefficients in time and space
B_1, B_2	=	number of blades in inlet guide vane and rotor rows
c	=	chord
$\mathbf{D}$	=	pseudo-spectral operator
$\mathbf{E}$, $\mathbf{E}^{-1}$	=	discrete Fourier and inverse Fourier transformation matrices
$\boldsymbol{F}$, $\boldsymbol{G}$, $\boldsymbol{H}$	=	flux vectors
N	=	nodal diameters
p	=	pressure
$\boldsymbol{S}$	=	source vector
t	=	time
$\boldsymbol{U}$	=	vector of conservation variables
$\boldsymbol{U}^*$	=	vector of conservation variables in all subtime levels
$\tilde{\boldsymbol{U}}$	=	vector of Fourier coefficients
x, y, z	=	Cartesian coordinates
x, θ, r	=	relative cylindrical coordinates
θ_G	=	blade-to-blade gap
σ	=	interblade phase angle
τ	=	pseudo-time
Ω	=	wheel speed
ω	=	excitation frequency

Presented as Paper 1240 at the 47th AIAA Aerospace Sciences Meeting including The New Horizons Forum and Aerospace Exposition, Orlando, FL, 5–8 January 2009; received 17 February 2009; revision received 1 December 2009; accepted for publication 3 December 2009.

*Assistant Professor, Department of Mechanical, Aerospace, and Biomedical Engineering. Senior Member AIAA.
†Julian Francis Abele Professor, Department of Mechanical Engineering and Materials Science. Associate Fellow AIAA.
‡Associate Chair, Department of Mechanical Engineering and Materials Science. Senior Member AIAA.

I. Introduction

BLADE row interactions in multistage turbomachinery play a vital role in the overall aerodynamic and aeromechanical performance of modern gas turbine engines [1–6]. Therefore, the accurate prediction of such interactions is critically important as such predictions can improve the fundamental understanding of complex flow physics, reduce development time, and more important, reduce the occurrence of engine failures. In the past three decades, with the advancement in the computer technology, increasingly sophisticated computer fluid dynamic models of unsteady flows that involve blade row interactions have been developed. Most of these numerical models were based on time-accurate methods, which are well documented in the literature [7–11]. In general, the unsteady flow calculations in multistage turbomachinery using direct time simulation techniques are very expensive in terms of both computational time and memory storage. If the blade counts for neighboring blade rows are different, then it may be necessary to model multiple passages, or even the whole annulus of the domain, increasing the computational time and storage. Also, depending on the temporal discretization used, several solutions at previous time steps must be stored, thereby increasing the memory requirements. These requirements put an increased pressure on the industry as the gas turbine design cycle is getting more and more compressed.

To reduce such computational and memory requirements, and to improve the accuracy of unsteady flow models, investigators have developed efficient nonlinear frequency-domain techniques. The harmonic balance method, a computationally efficient technique, was first used by Hall et al. [12,13] for the analysis of nonlinear flows in turbomachinery. In recent years, a number of investigators have contributed to the development of the harmonic balance technique, or have used the technique to solve interesting physical problems [14–22]. Using this approach, the unsteady flow is assumed to be temporally periodic, a condition satisfied for many unsteady flows of

interest. The flow conservation variables are stored at a number of subtime levels over one temporal period. The time derivative term in the conservation equations (Euler or Navier–Stokes) is replaced by a time-spectral operator that is proportional to the fundamental frequency of the unsteadiness, eliminating the explicit dependence on time from the governing equations. Finally, the solution at multiple subtime levels are obtained using standard steady flow computational fluid dynamics (CFD) techniques.

The main advantages of the harmonic balance approach compared with a time-accurate method are its computational efficiency and its ability to more accurately model certain parts of the unsteady flow problem. For instance, the specification of both far-field and periodic boundary conditions are greatly simplified in the frequency domain. Complex periodicity conditions allow one to reduce the computational domain to a single blade passage in each row of a turbomachine, greatly reducing the computational cost. On the other hand, the main disadvantage of the harmonic balance approach is the increased memory requirement due to the storage of different time level solutions.

Recently, Ekici and Hall [23,24] have developed a variation of the harmonic balance technique that can model unsteady flows in multistage turbomachinery. In that earlier work, the source of the flow unsteadiness was blade vibration (the flutter problem) and relatively weak pressure disturbances associated with the mean circumferential pressure variation associated with subsonic flow through a compressor blade row. This paper investigates whether the harmonic balance technique can model multistage flows with strong blade row interactions. In particular, we compare the results of the harmonic balance analysis to the experimental results presented by Richman and Fleeter [1], who examined the interaction of strong shocks propagating upstream of a compressor rotor and impinging on the upstream inlet guide vane. Such upstream propagating shocks can cause large unsteady forcing on the blade rows, potentially resulting in high-cycle-fatigue failure. In this paper we also examine the convergence of the harmonic balance method with increasing number of time levels (Fourier modes) retained in the computational model and demonstrate that the current approach predicts accurately the unsteady pressures, which can be used in a subsequent forced response analysis. Furthermore, we show that the unsteadiness is well modeled with a modest number of subtime levels. To the best of our knowledge, this is the first paper in the literature that presents a detailed comparison of the harmonic balance method to experimental data for a strongly nonlinear shock/vane interaction problem.

II. Flowfield Kinematics

The details of the harmonic balance technique used in this work was previously presented by Ekici and Hall [24]. For completeness, the salient features of that analysis are presented here.

Consider the case where two blade rows operate in close proximity to one another, as in the case of an inlet guide vane (IGV) and first rotor. Suppose there are B_1 blades in the IGV row, and B_2 blades in the rotor row. In the absence of blade vibration or some other external forcing mechanism, the flow between the blade rows can be decomposed into a Fourier series in the circumferential direction. The flow will have N nodal diameters so that

$$N = lB_1 + mB_2 \tag{1}$$

where l and m can take on all integer values. In the rotor frame of reference, the temporal frequency of the unsteadiness of a particular nodal diameter mode will be

$$\omega = -lB_1\Omega \tag{2}$$

where Ω is the rotational speed of the rotor. Similarly, in the IGV frame of reference the frequency is given by

$$\omega' = mB_2\Omega \tag{3}$$

These discrete frequencies represent the possible frequencies that will appear in the flow (absent any self-induced flow unsteadiness or subharmonics). Therefore, the flow in the rotor, for example, may be represented by the time series

$$\boldsymbol{U}(x,r,\theta,t) = \sum_l \sum_m [\tilde{\boldsymbol{A}}_{lm}(x,r)\cos(\omega_{lm}t + N_{lm}\theta) + \tilde{\boldsymbol{B}}_{lm}(x,r)\sin(\omega_{lm}t + N_{lm}\theta)] \tag{4}$$

or more generally

$$\boldsymbol{U}(x,r,\theta,t) = \boldsymbol{A}_0(x,r,\theta) + \sum_{k=1}^{K} [\boldsymbol{A}_k(x,r,\theta)\cos(\omega_k t) + \boldsymbol{B}_k(x,r,\theta)\sin(\omega_k t)] \tag{5}$$

where now ω_k is the kth nonrepeated nonzero frequency and $\boldsymbol{A}_k$ and $\boldsymbol{B}_k$ are the Fourier coefficients of mode k.

In the present computational method, we store the conservation variables in each blade row at a number of subtime levels. Assembled together into one vector, these solutions are denoted by the vector $\boldsymbol{U}^*$. We denote the vector of Fourier coefficients by $\tilde{\boldsymbol{U}}$, that is,

$$\boldsymbol{U}^* = \begin{Bmatrix} \boldsymbol{U}_1 \\ \boldsymbol{U}_2 \\ \boldsymbol{U}_3 \\ \vdots \end{Bmatrix}, \qquad \tilde{\boldsymbol{U}} = \begin{Bmatrix} \boldsymbol{A}_0 \\ \boldsymbol{A}_1 \\ \vdots \\ \boldsymbol{B}_1 \\ \vdots \end{Bmatrix} \tag{6}$$

For temporally periodic flows, the Fourier coefficients can be determined from the subtime level solutions by a discrete Fourier transform. Conversely, the conservation variables at the subtime level can be determined from the Fourier coefficients by the inverse discrete Fourier transform. These relations can be written in matrix form as

$$\tilde{\boldsymbol{U}} = \mathbf{E}\boldsymbol{U}^* \tag{7}$$

$$\boldsymbol{U}^* = \mathbf{E}^{-1}\tilde{\boldsymbol{U}} \tag{8}$$

where $\mathbf{E}$ is the discrete Fourier transform operator written in matrix form. $\mathbf{E}$ is a square matrix as the number of time sublevels is equal to the number of Fourier coefficients. Note that in our computational code, we store $\boldsymbol{U}^*$ as our working variable, and only compute $\tilde{\boldsymbol{U}}$ at the computational boundaries when applying periodic, far-field, and interrow connectivity boundary conditions.

III. Harmonic Balance Equations

Having described the kinematics of the flow, we now turn our attention to the development of the harmonic balance equations. Here, we consider the Euler equations for simplicity, although our computer code is implemented for the Navier–Stokes equations. In conservation form, the Euler equations in relative frame of reference may be written as

$$\frac{\partial \boldsymbol{U}}{\partial t} + \frac{\partial \boldsymbol{F}}{\partial x} + \frac{\partial \boldsymbol{G}}{\partial y} + \frac{\partial \boldsymbol{H}}{\partial z} = \boldsymbol{S} \tag{9}$$

Note that Eq. (9) contains five equations: one conservation of mass equation, three conservation of momentum equations, and one conservation of energy equation. Next, we write these equations at all subtime levels simultaneously, so that

$$\frac{\partial \boldsymbol{U}^*}{\partial t} + \frac{\partial \boldsymbol{F}^*}{\partial x} + \frac{\partial \boldsymbol{G}^*}{\partial y} + \frac{\partial \boldsymbol{H}^*}{\partial z} = \boldsymbol{S}^* \tag{10}$$

where, for example, $\boldsymbol{F}^*$ is the vector of x fluxes evaluated at $\boldsymbol{U}^*$. Hence, Eq. (10) has $5 \times M$ equations, where M is the number of subtime levels.

Note that the M sets of conservation equations in Eq. (10) are coupled only through the time derivative term, which is approximated by the pseudospectral operator $\mathbf{D}$ given by

$$\frac{\partial \boldsymbol{U}^*}{\partial t} = \frac{\partial \mathbf{E}^{-1}}{\partial t}\mathbf{E}\boldsymbol{U}^* = \mathbf{D}\boldsymbol{U}^* \tag{11}$$

Finally, substitution of Eq. (11) into Eq. (10) gives the desired harmonic balance equations, that is,

$$\mathbf{D}\,\boldsymbol{U}^* + \frac{\partial \boldsymbol{F}^*}{\partial x} + \frac{\partial \boldsymbol{G}^*}{\partial y} + \frac{\partial \boldsymbol{H}^*}{\partial z} = \boldsymbol{S}^* \tag{12}$$

To solve the harmonic balance equations, we introduce a pseudotime term so that the equations may be marched rapidly to a steady-state condition using a conventional CFD scheme. Thus, Eq. (12) becomes

$$\frac{\partial \boldsymbol{U}^*}{\partial \tau} + \mathbf{D}\boldsymbol{U}^* + \frac{\partial \boldsymbol{F}^*}{\partial x} + \frac{\partial \boldsymbol{G}^*}{\partial y} + \frac{\partial \boldsymbol{H}^*}{\partial z} = \boldsymbol{S}^* \tag{13}$$

where τ is fictitious or pseudotime, used only to march Eq. (13) to steady state, driving the pseudotime term to zero. Note that pseudotime harmonic balance equations are similar in form to the original time-domain form of the Euler equations. Thus, existing well-developed steady CFD techniques may be used to efficiently solve the nonlinear harmonic balance equations, with comparable number of iterations required.

In the present work, we use a Lax–Wendroff [25] flow solver to discretize and solve the pseudotime for the harmonic balance equation, Eq. (13).

IV. Periodicity Boundary Conditions

The computational domain can be reduced to a single blade passage within each blade row by making use of complex periodicity conditions along the periodic boundaries. To apply these conditions, the solution $\boldsymbol{U}^*$ is transformed along the periodic boundaries using Eq. (7) to find the vector of Fourier coefficients $\tilde{\boldsymbol{U}}$ (which contains the cosine and sine coefficients $\boldsymbol{A}_k$ and $\boldsymbol{B}_k$). Inspection of Eq. (5) reveals that the appropriate boundary conditions are given by

$$\boldsymbol{A}_k(x, r, \theta + \theta_G) = \boldsymbol{A}_k(x, r, \theta) \cdot \cos(N_k\theta_G) - \boldsymbol{B}_k(x, r, \theta) \cdot \sin(N_k\theta_G) \tag{14}$$

$$\boldsymbol{B}_k(x, r, \theta + \theta_G) = \boldsymbol{A}_k(x, r, \theta) \cdot \sin(N_k\theta_G) + \boldsymbol{B}_k(x, r, \theta) \cdot \cos(N_k\theta_G) \tag{15}$$

These boundary conditions, similar to those developed by He and Denton [26] and He [27] for time-accurate time-marching flow solvers, are applied at every iteration of the Lax–Wendroff solver.

V. Multistage Coupling

At each iteration of the harmonic balance scheme, the solutions along the interrow boundaries of the computational grids are matched to one another. The process is as follows. The subtime level solutions $\boldsymbol{U}^*$ along the interrow boundaries of the IGV and rotor passages are Fourier transformed in time using Eq. (7) to compute the temporal Fourier coefficients $\boldsymbol{A}_k$ and $\boldsymbol{B}_k$. Next, a spatial Fourier transform in the circumferential direction is performed on these coefficients to obtain the Fourier coefficients $\tilde{\boldsymbol{A}}_{lm}$ and $\tilde{\boldsymbol{B}}_{lm}$. These coefficients are then matched across the interrow boundaries. This matching is done for each circumferential mode originally hypothesized as one of the (l, m) modes present in the solution. To eliminate spurious reflections off the interrow boundaries, two-dimensional nonreflecting boundary conditions are applied to those possible circumferential modes not included in the hypothesized mode set. Thus, these higher circumferential modes pass out of the computational domain and simply disappear, that is, the outgoing waves do not influence the solution in the neighboring blade row, nor are they reflected.

Once the matching and nonreflecting boundary conditions have been applied to the Fourier coefficients $\tilde{\boldsymbol{A}}_{lm}$ and $\tilde{\boldsymbol{B}}_{lm}$, a spatial inverse Fourier transform is performed to find the temporal Fourier coefficients ($\boldsymbol{A}_k$ and $\boldsymbol{B}_k$) at each circumferential node location along the interrow interface. Finally, a temporal inverse Fourier transform is performed [Eq. (8)] to determine the conservation variables $\boldsymbol{U}^*$ at each subtime level.

VI. Numerical Results

In this paper, we demonstrate the use of harmonic balance technique to model the nonlinear blade row interaction phenomenon in multistage turbomachinery. Specifically, we consider the first two rows (IGV/rotor) of the Purdue Transonic Multistage Research Compressor. The IGV blades have control diffusion airfoil profiles, whereas the rotor blades have NACA 65 series profiles. The blade counts for the IGV and the rotor rows are 18 and 19, respectively. For the IGV blade row, experimental data is available at the compressor design speed of 20,000 RPM. At design conditions the inlet Mach number and the compressor total pressure ratio are 0.35 and 1.32, respectively. The transonic rotor operates at a supersonic relative velocity with a shock formation on the suction side of the blade. The shock propagates upstream and interacts with the IGV blade row with the potential of causing high-cycle fatigue failure. Further details about the geometry and the flow conditions can be found in a paper written by Richman and Fleeter [1]; unsteady surface pressure and PIV data are presented at 90% span location.

A. Grid Convergence

Before any detailed unsteady computations are carried out, a grid convergence study is performed to ensure the grid independence of

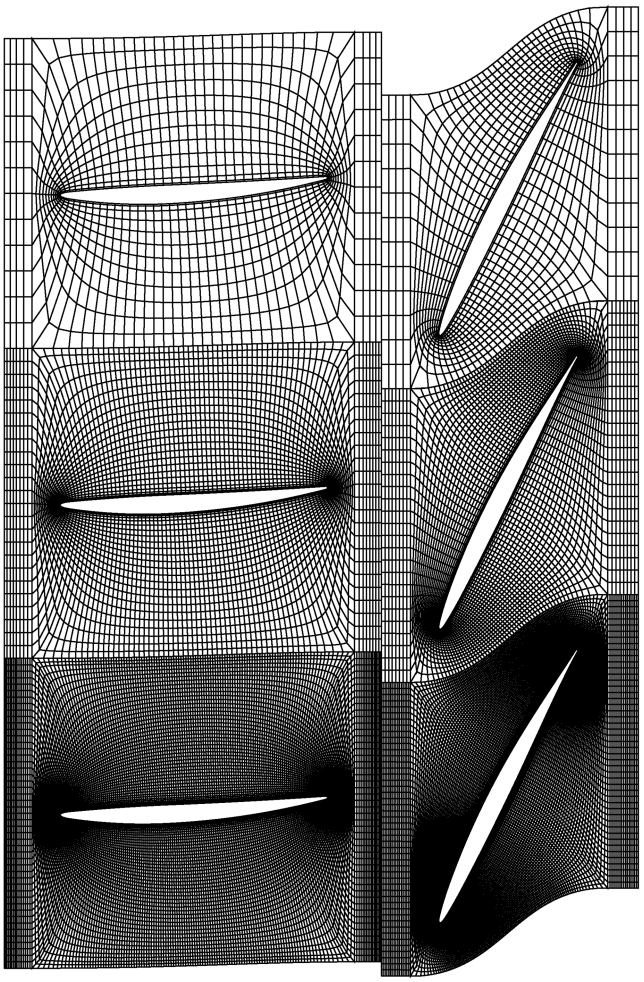

Fig. 1 Computational grids used for grid convergence study. Top represents the coarse grid, middle represents the medium grid, and bottom represents the fine grid.

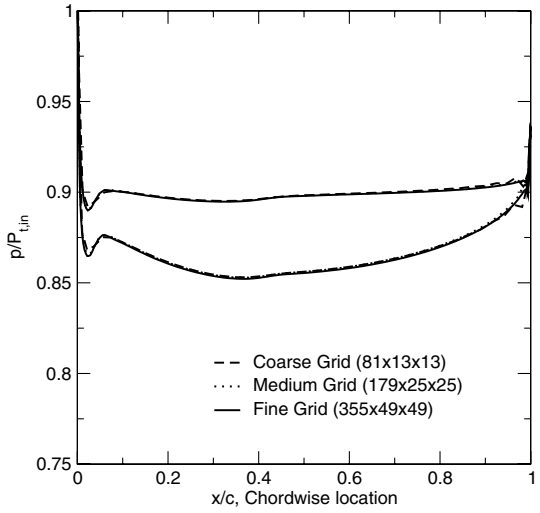

Fig. 2 Steady pressure distribution at 90% span of the IGV blades using the fine, medium, and coarse grids.

the inviscid steady computations. Note that although a similar grid convergence study was performed for the viscous grid used in this paper, we only consider the inviscid grids in this section. To begin, three grids with different resolutions ($355 \times 49 \times 49$, $179 \times 25 \times 25$, and $81 \times 13 \times 13$ nodes) are generated for each blade row. For comparison, Fig. 1 shows the inviscid computational grids at 90% span at different passages. Note that using the harmonic balance technique and complex periodic boundary conditions, the computational domain is reduced to a single blade passage in each blade row. In comparison, a typical dual time-stepping time-accurate solver would need to model the entire wheel for both blade rows since the number of blades in the two blade rows have no common divisors.

To assess the quality of the grids, we compare the surface pressure distributions obtained for inviscid computations at the 90% span of the IGV blade row. As can be seen from Fig. 2, the differences between the fine and the medium grid solutions are indistinguishable whereas a slight but visible difference exists for the coarse grid near the leading and the trailing edges. Although not presented here, a detailed comparison of the entire flowfield for these grids was performed and grid convergence was achieved for the inviscid computations using the medium grid ($179 \times 25 \times 25$ nodes). Similarly, a $211 \times 49 \times 49$ node grid was found to be adequate for viscous computations.

B. Steady Flowfield

Next, the steady flow through the multirow configuration is computed without any unsteady excitation, that is, $(l, m) = (0, 0)$.

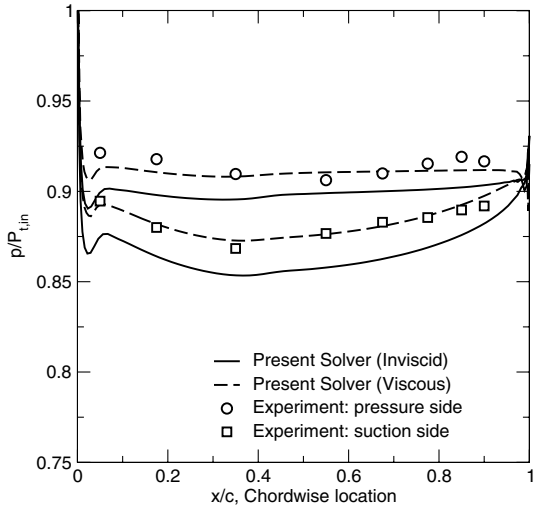

Fig. 3 Steady pressure distribution at 90% span of the IGV blades.

Shown in Fig. 3 is the computed pressure distributions as well as the experimental data as reported by Richman and Fleeter [1] on the blade surface at 90% span of the IGV row. As can be seen, the predicted surface pressure values for the inviscid computations are lower than the experimentally measured values. This is mainly due to the fact that the predicted shock location in the rotor row is further downstream of the actual shock location, which affects the pressure field in the IGV blade row. However, the viscous computations are in better agreement with the experiments. We must note that the viscous computations did not include a tip-clearance gap, and flow tangency boundary conditions were used at the hub and tip walls.

Figure 4 shows the static pressure contour plots at 90% span for the steady computations. Note the complex shock structure in the rotor blade row for both viscous and inviscid calculations. It is clear that the captured shock is further downstream for the inviscid case, which results in lower pressure on the IGV blade surface compared with the experimental data. Also note that because only one mode is retained, which is equivalent to a steady mixing-plane computation, the pressure contours do not match at the interrow boundary and the shock wave cannot propagate upstream. However, the circumferential average of the pressure values are matched in both cases.

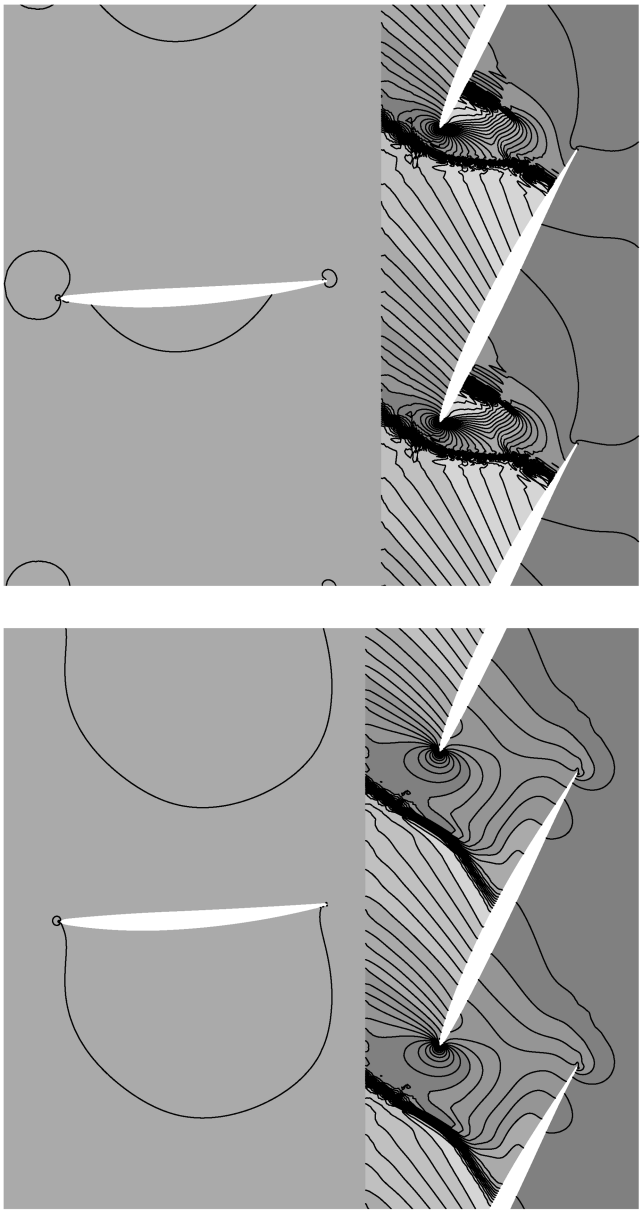

Fig. 4 Steady pressure contours at 90% span. Top represents inviscid, and bottom represents viscous.

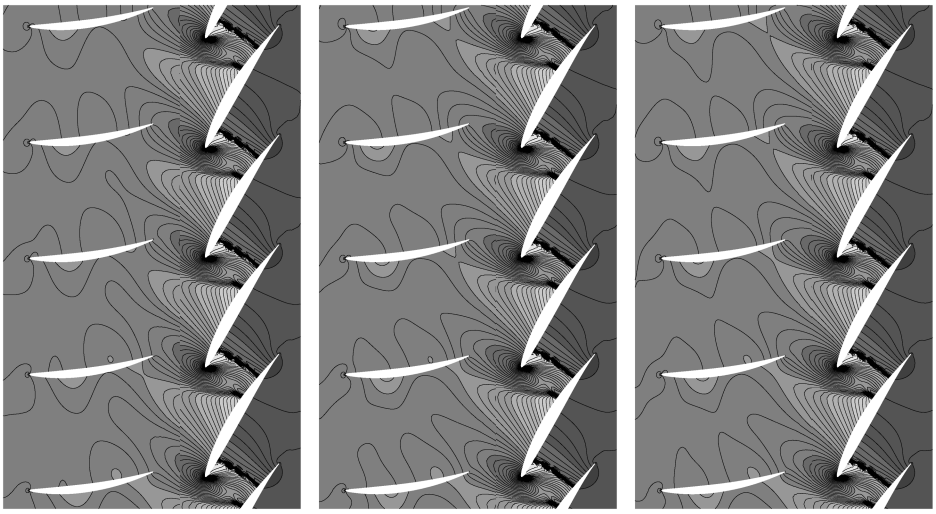

Fig. 5 Instantaneous unsteady pressure contours at 30% span. Left shows 4-mode solution, middle shows 9-mode solution, and right shows 16-mode solution.

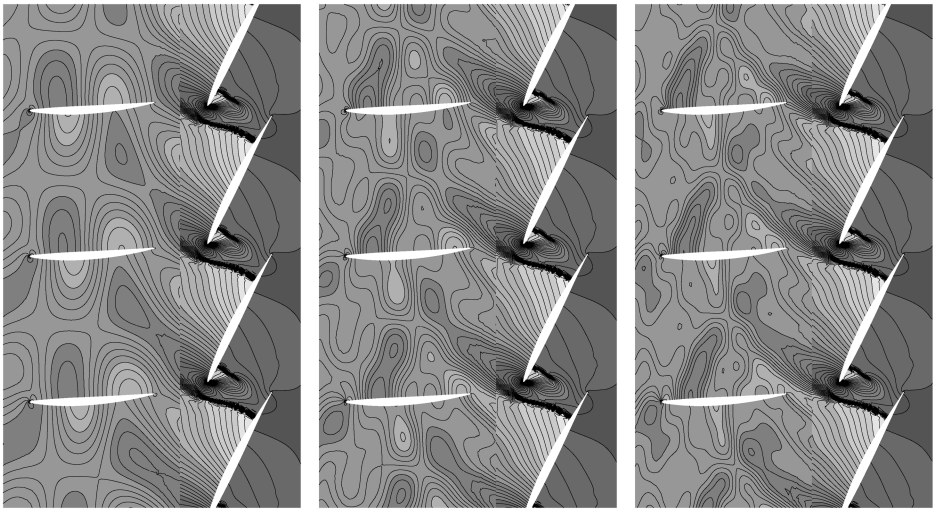

Fig. 6 Instantaneous unsteady pressure contours at 90% span. Left shows 4-mode solution, middle shows 9-mode solution, and right shows 16-mode solution.

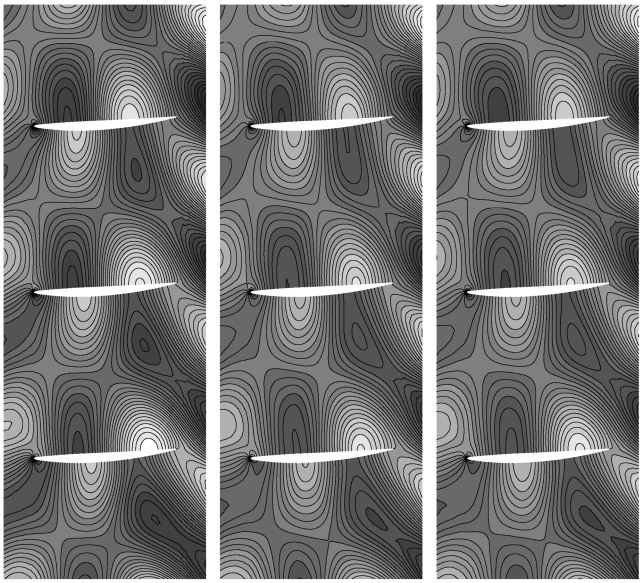

Fig. 7 First harmonic of unsteady pressure at 90% span. Left shows 4-mode solution, middle shows 9-mode solution, and right shows 16-mode solution.

C. Inviscid Unsteady Flowfield

Next, we use the present method to compute the inviscid unsteady flowfield. As mentioned previously, before any unsteady computation one needs to select a set of modes associated with the indices (l, m) and compute the discrete frequencies and interblade phase angles for each blade row. For this case, three different unsteady runs were performed. In the first run, a total of four modes were retained, which resulted in a single blade passing frequency, or equivalently, three subtime level solutions in each blade row. Similarly, for runs two and three, 9 and 16 modes were retained in the unsteady computation, which resulted in two and three discrete nonzero frequencies, respectively.

Shown in Fig. 5 are the unsteady pressure contours at 30% span for 4, 9, and 16 modes. As can be seen, the unsteady pressure waves propagate upstream of the rotor blade row. The pressure contours match relatively well at the interrow boundary for 4- and 9-mode computations, whereas they match perfectly for the 16-mode model. In addition, the unsteady flow in the rotor row is nearly unchanged for all solutions; the blade row coupling effects are more pronounced for the IGV blade row.

We now consider the solutions at 90% span, a location for which there is experimental data available. Shown in Fig. 6 are the unsteady pressure contours for this spanwise location. It can be seen that unlike the solutions at 30% span, the unsteady solutions do not match well at the interrow boundary when four modes are retained in the model. It

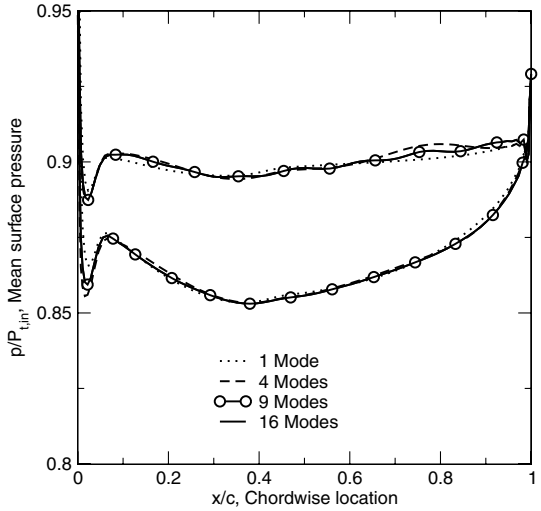

Fig. 8 Mean surface pressure distribution at 90% span of the IGV blades.

is obvious that a single harmonic is not adequate to pass the shock wave smoothly across the interrow interface. However, the quality of the solution improves as the number of modes, and hence the number of harmonics, is increased and the unsteady solutions clearly match better at the interrow boundary.

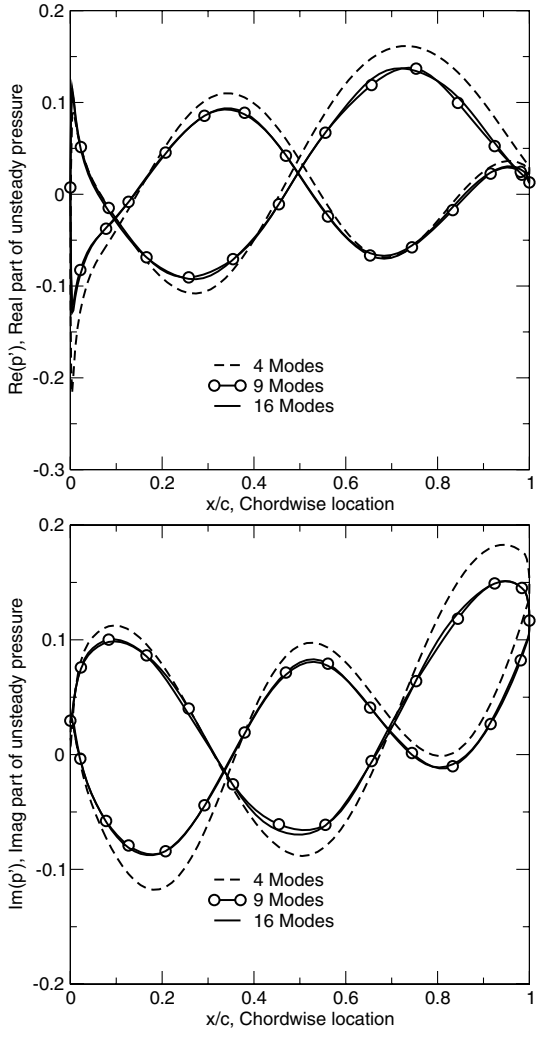

Fig. 9 Unsteady surface pressure distribution at 90% span of the IGV blades.

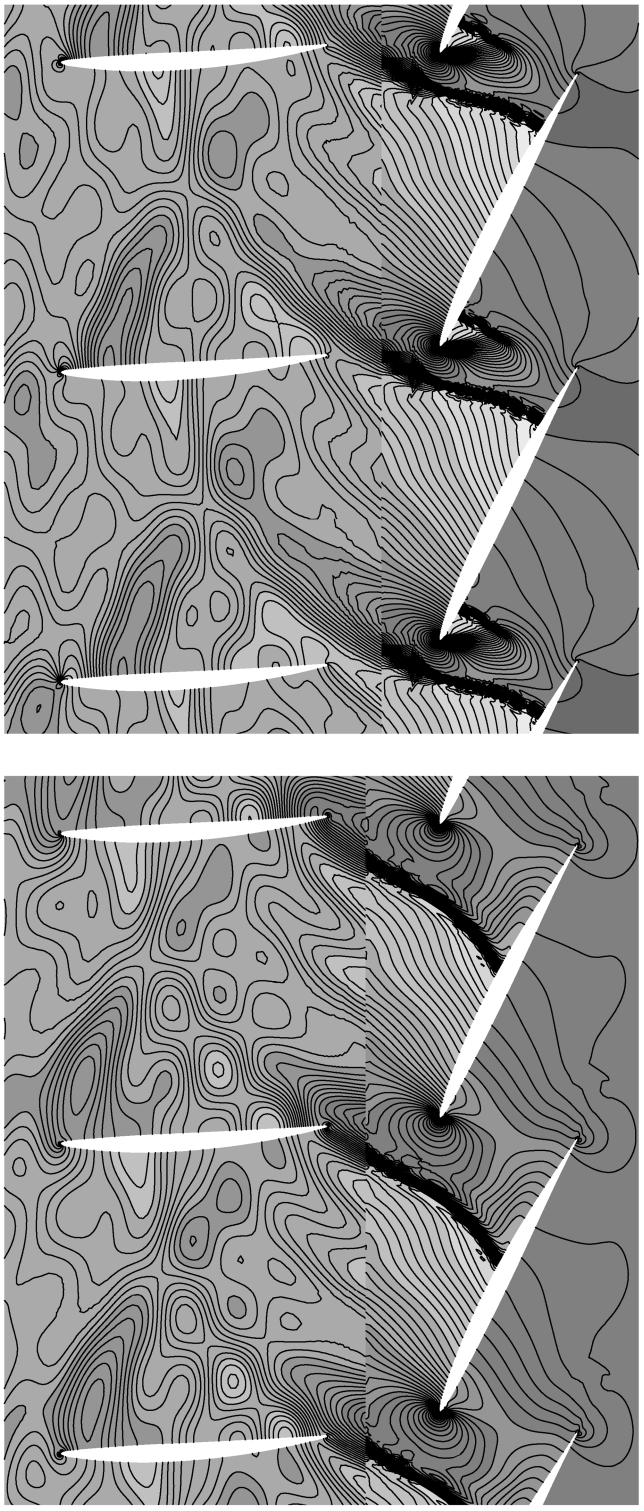

Fig. 10 Unsteady pressure flowfield at 90% span of the IGV blades. Top represents inviscid, and bottom represents viscous.

D. Mode Convergence

Up to this point, we have presented inviscid unsteady results in the time domain, computed by summing all terms retained in the Fourier series. However, often it is important to predict accurately only one or a very few of the Fourier coefficients of the unsteady flow. For example, if one needed to calculate the forced response of a blade row at a natural frequency near the first harmonic, then it is only the first harmonic of the unsteady pressure (or more precisely the generalized force) that is important. As an example, Fig. 7 shows contours of the first harmonic of unsteady pressure within the inlet guide vane passages computed using 4, 9, and 16 modes (corresponding to

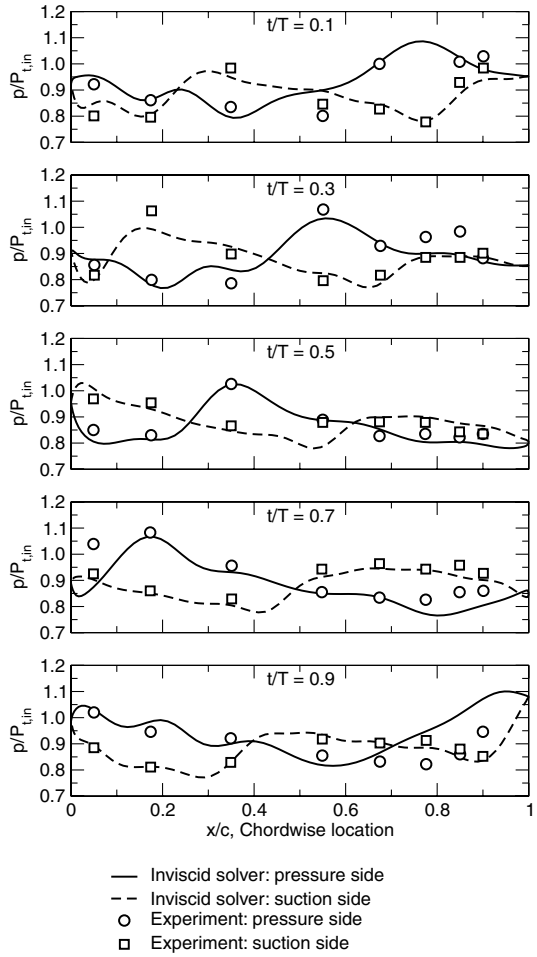

Fig. 11 Unsteady pressure over one rotor passing period at 90% span of the IGV blades (inviscid).

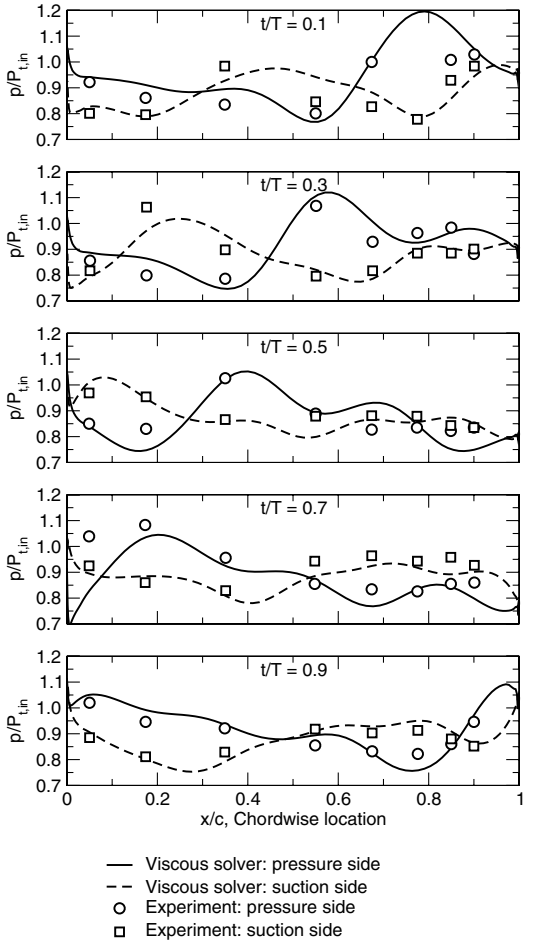

Fig. 12 Unsteady pressure over one rotor passing period at 90% span of the IGV blades (viscous).

frequencies one, two, or three times the rotor passing frequency). We note that all three solutions are very similar, with the 9- and 16-mode solutions being almost indistinguishable. Thus, the first harmonic of unsteady pressure is mode-converged with just nine modes, even though higher harmonics may not be mode-converged.

Next, we plot the mean pressure on the blade surface at 90% span when 4, 9, and 16 modes are kept for unsteady computations (see Fig. 8). Also shown in the same figure is the pressure distribution for the multirow steady solution. It is clear that although the differences are small, the mean (time-averaged) surface pressure obtained from the unsteady computations is different than the one obtained from the steady computation. This clearly indicates a nonlinear effect, and for the purpose of computing mean flow quantities nonlinear interactions of unsteadiness in the flow may be important. Also note that as the number of modes are increased, the mean pressure solution converges to a fixed value. Next, we investigate the effect of number of modes on the unsteady pressure at the rotor passing frequency. Shown in Fig. 9 are the real and imaginary parts of the first harmonic of the unsteady pressure. The mode convergence can clearly be seen as the number of modes is increased and all three computations capture the unsteady effects quite well. These results indicate one only needs as few as four modes for engineering accuracy, and only nine modes to obtain mode-converged solutions at rotor passing frequency.

E. Solver Accuracy

Having investigated the effect of the number of modes retained in the model for inviscid computations, we now compare our viscous and inviscid solutions. Figure 10 shows the calculated contour plots of pressure when 16 modes are retained in the model. As expected, the viscous and inviscid flowfield solutions differ significantly in the rotor, with the shock sitting further forward in the viscous solution. However, in both cases the shock propagates upstream and impinges on the IGV blades, forming a lambda structure in the IGV. Overall, the viscous and inviscid solutions seem to be in better agreement in the IGV blade row, although there are minor but visible differences in both solutions. The presence of the shock in the IGV is due entirely to the propagation of the shock emanating from the rotor. Its interaction with the IGV is highly dynamic, with unsteady refections off of the IGV blade surfaces. Such dynamic shock interactions are, perhaps, less dependent on viscous effects.

Next we compare our inviscid and viscous calculations to experimental data presented by Richman and Fleeter [1]. Shown in Figs. 11 and 12 are the computed unsteady surface pressure distributions at 90% span location of the IGV blade row for the inviscid and viscous computations, respectively, together with the experimental data. The computed results correspond to the 16-mode (seven subtime level) runs. One can see that overall the agreement between the numerical results and the experimental data is good. Both inviscid and viscous solutions capture the amplitude and the phase of the unsteady pressure wave reasonably well for all time instances over a single period. Finally, we compare the instantaneous Mach number contours obtained using the current unsteady analysis with the available PIV [1] data (see Fig. 13). As can be seen, our results are in good qualitative agreement with the measurements performed at Purdue University. Similar flow features were reported by Richman and Fleeter [1] and Silkowski et al. [2] using time-accurate solvers. However, in both papers a one-to-one blade count was used to avoid high computational and memory requirements of the time-accurate solution. No such simplifications were made in this paper. Note, however, the appearance of small islands of contours and a general "waviness in the computed solution. The shocks, for example, appear smeared and irregular. This is because the harmonic

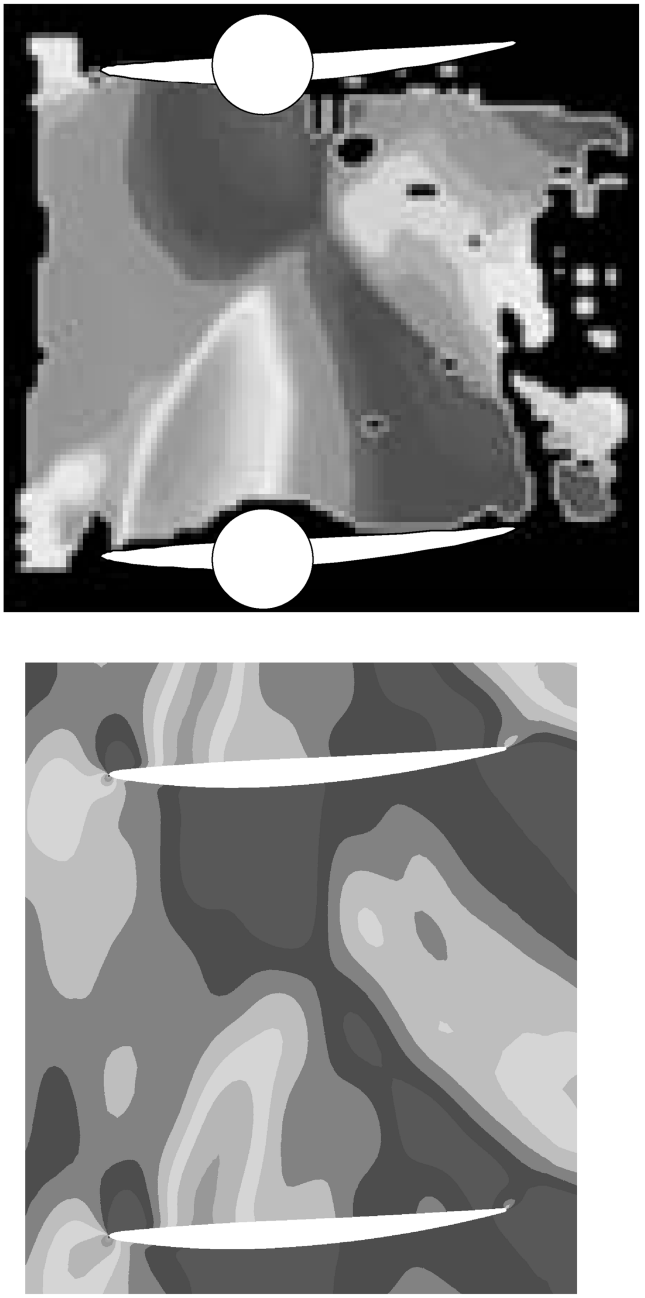

Fig. 13 Instantaneous Mach contours at 90% span. Top shows Purdue PIV data [1] (used with permission). Bottom shows present computation.

balance solution is designed to compute the lower harmonics of the unsteady flow accurately; detailed instantaneous flow features can be resolved, but only if more subtime levels (harmonics) are included in the model. Nevertheless, the solution shown predicts accurately the mean flow and unsteady flow associated with the fundamental excitation frequency.

F. Computational Efficiency

Having computed the unsteady flow, we return to the issue of computational efficiency of the present method. Figure 14 shows the convergence histories for the present harmonic balance method with seven subtime level solutions (16 modes) and for the steady flow solver (1 mode). Note that in both cases the terminal convergence rates of the two solutions are the same. Thus, because the computation time scales linearly with the number of subtime levels, the computational time required for unsteady computation is approximately equal to seven times the computational time required for a single steady flow calculation. The present method also benefits

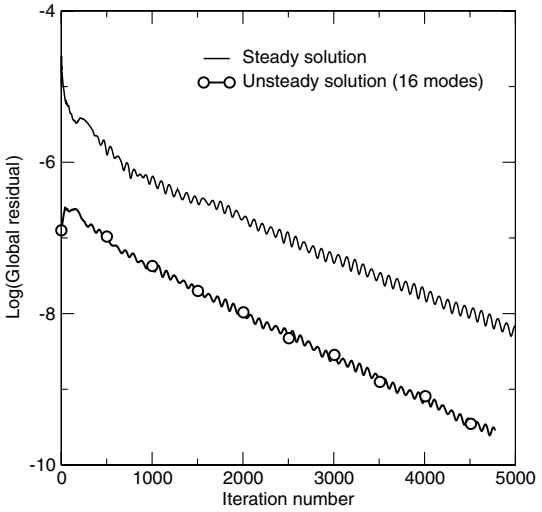

Fig. 14 Convergence history.

greatly from the fact that only a single blade passage is required in each blade row, and from the fact that only a small number of subtime levels are needed to obtain accurate solutions.

VI. Conclusions

An important component of vane and blade design is the analysis of the vane/blade excitation problem. Industry needs fast and accurate methods to predict the resonant response amplitudes. The most difficult and time-consuming part of such analysis is the determination of unsteady pressures due to the blade row interactions. In this paper, we have presented an efficient harmonic balance technique for computing strongly nonlinear blade row interaction problems in turbomachinery.

The present method was applied to the problem of IGV/rotor interaction and was found to predict accurately the complex unsteady flowfield associated with transonic IGV/rotor shock interaction. In particular, we have shown that the first harmonic of the unsteady pressure on the surface of the inlet guide vanes is accurately predicted with a modest number of harmonics (time levels), with only one to two harmonics (three to five time levels) giving converged solutions that are in good agreement with the experiment. We believe this is the first work in the literature to compare results for shock/vane interactions obtained from a multistage harmonic balance analysis to experimental data.

In addition, we have found the harmonic balance method to be very computationally efficient, mainly for three reasons. First, the computational domain can be reduced to a single blade passage regardless of the blade counts. Second, time derivatives are computed using a very accurate spectral operator, reducing the number of time levels that must be retained in the model. And third, because the time derivative in the Euler or Navier–Stokes equation is replaced by a time-spectral operator, the explicit dependence on time is eliminated, and very powerful convergence acceleration techniques originally developed for steady flow problems can be used to speed convergence. With these computational savings, nonlinear harmonic balance analysis of unsteady flow investigated in this paper takes between three and seven times the computational time required for a steady flow computation.

Acknowledgment

This work was sponsored by a grant from the GUIde Consortium.

References

[1] Richman, M., and Fleeter, S., "Navier–Stokes Simulation of IGV-Rotor-Stator Interactions in a Transonic Compressor," AIAA Paper 2000-3379, 2000.

[2] Silkowski, P. D., Rhie, C. M., Copeland, G. S., Eley, J. A., and Bleeg, J. M., "Computational-Fluid-Dynamics Investigation of Aeromechanics," *Journal of Propulsion and Power*, Vol. 18, No. 4, July 2002, pp. 788–796. doi:10.2514/2.6001

[3] Bakhle, M. A., Liu, J. S., Panovsky, J., Keith, T. G., and Mehmed, O., "Calculation and Correlation of the Unsteady Flowfield in a High-Pressure Turbine," American Society of Mechanical Engineers, Paper GT-2002-30322, 2002.

[4] Gorrell, S. E., Car, D., Puterbaugh, S. L., Estevadeordal, J., and Okiishi, T. H., "An Investigation of Wake-Shock Interactions in a Transonic Compressor With Digital Particle Image Velocimetry and Time-Accurate Computational Fluid Dynamics," *Journal of Turbomachinery*, Vol. 128, No. 4, Oct. 2006, pp. 616–626. doi:10.1115/1.2220049

[5] Vahdati, M., Sayma, A. I., Imregun, M., and Simpson, G., "Multibladerow Forced Response Modeling in Axial-Flow Core Compressors," *Journal of Turbomachinery*, Vol. 129, No. 2, April 2007, pp. 412–420. doi:10.1115/1.2436892

[6] Van Zante, D., Chen, J. P., Hathaway, M., and Chriss, R., "The Influence of Compressor Blade Row Interaction Modeling on Performance Estimates From Time-Accurate, Multistage, Navier-Stokes Simulations," *Journal of Turbomachinery*, Vol. 130, No. 1, Jan. 2008, pp. 1–10.

[7] Denton, J. D., "The Calculation of Three Dimensional Viscous Flow Through Multistage Turbomachinery," American Society of Mechanical Engineers, Paper 90-GT-19, 1990.

[8] Chen, J. P., and Whitfield, D. L., "Navier–Stokes Calculations for the Unsteady Flowfield of Turbomachinery," AIAA Paper 93-0676, 1993.

[9] Chen, J. P., Celestina, M. L., and Adamczyk, J. J., "New Procedure for Simulating Unsteady Flows Through Turbomachinery Blade Passages," American Society of Mechanical Engineers, Paper 94-GT-151, 1994.

[10] Volmar, T. W., Brouillet, B., and Gallus, H. E., "Time-Accurate Three-Dimensional Navier–Stokes Analysis of One-and-One-Half Stage Axial-Flow Turbine," *Journal of Propulsion and Power*, Vol. 16, No. 2, 2000, pp. 327–335. doi:10.2514/2.5573

[11] Chaluvadi, V. S. P., Kalfas, A. I., Banieghbal, M. R., Hodson, H. P., and Denton, J. D., "Blade-Row Interaction in a High-Pressure Turbine," *Journal of Propulsion and Power*, Vol. 17, No. 4, 2001, pp. 892–901. doi:10.2514/2.5821

[12] Hall, K. C., Thomas, J. P., and Clark, W. S., "Computation of Unsteady Nonlinear Flows in Cascades Using a Harmonic Balance Technique," *Proceedings of the 9th International Symposium on Unsteady Aerodynamics, Aeroacoustics, and Aeroelasticity of Turbomachines*, edited by P. Ferrand and S. Aubert, Presses Universitaires de Grenoble, Lyon, France, Sept. 2000, pp. 409–426.

[13] Hall, K. C., Thomas, J. P., and Clark, W. S., "Computation of Unsteady Nonlinear Flows in Cascades Using a Harmonic Balance Technique," *AIAA Journal*, Vol. 40, No. 5, May 2002, pp. 879–886. doi:10.2514/2.1754

[14] Chen, T., Vasanthakumar, P., and He, L., "Analysis of Unsteady Blade Row Interaction Using Nonlinear Harmonic Approach," *Journal of Propulsion and Power*, Vol. 17, No. 3, May–Jun. 2001, pp. 651–658. doi:10.2514/2.5792

[15] McMullen, M., Jameson, A., and Alonso, J. J., "Acceleration of Convergence to a Periodic Steady State in Turbomachinery Flows," AIAA Paper 2001–152, 2001.

[16] McMullen, M., Jameson, A., and Alonso, J. J., "Application of a Non-Linear Frequency Domain Solver to the Euler and Navier–Stokes equations," AIAA Paper 2002-120, 2002.

[17] Thomas, J. P., Dowell, E. H., and Hall, K. C., "Modeling Viscous Transonic Limit-Cycle Oscillation Behavior Using a Harmonic Balance Approach," *Journal of Aircraft*, Vol. 41, No. 6, Nov.–Dec. 2004, pp. 1266–1274. doi:10.2514/1.9839

[18] McMullen, M., Jameson, A., and Alonso, J., "Demonstration of Nonlinear Frequency Domain Methods," *AIAA Journal*, Vol. 44, No. 7, 2006, pp. 1428–1435. doi:10.2514/1.15127

[19] Vilmin, S., Lorrain, E., Hirsch, C., and Swoboda, M., "Unsteady Flow Modeling Across the Rotor/Stator Interface Using the Nonlinear Harmonic Method," American Society of Mechanical Engineers Paper GT2006-90210, 2006.

[20] Gopinath, A., van der Weide, E., Alonso, J. J., Jameson, A., Ekici, K., and Hall, K. C., "Three-Dimensional Unsteady Multi-Stage Turbomachinery Simulations using the Harmonic Balance Technique," AIAA Paper 2007-0892, 2007.

[21] Ekici, K., Hall, K. C., and Dowell, E. H., "Computationally Fast Harmonic Balance Methods for Unsteady Aerodynamic Predictions of Helicopter Rotors," *Journal of Computational Physics*, Vol. 227, No. 12, 2008, pp. 6206–6225. doi:10.1016/j.jcp.2008.02.028

[22] Ekici, K., and Hall, K. C., "Nonlinear Frequency-Domain Analysis of Unsteady Flows in Turbomachinery with Multiple Excitation Frequencies," *AIAA Journal*, Vol. 46, No. 8, Aug. 2008, pp. 1912–1920. doi:10.2514/1.26006

[23] Ekici, K., and Hall, K. C., "Nonlinear Analysis of Unsteady Flows in Multistage Turbomachines Using the Harmonic Balance Technique," AIAA Paper 2006-422, 2006.

[24] Ekici, K., and Hall, K. C., "Nonlinear Analysis of Unsteady Flows in Multistage Turbomachines Using Harmonic Balance," *AIAA Journal*, Vol. 45, No. 5, May 2007, pp. 1047–1057. doi:10.2514/1.22888

[25] Ni, R. H., "A Multiple-Grid Scheme for Solving the Euler Equations," *AIAA Journal*, Vol. 20, No. 11, Nov. 1982, pp. 1565–1571. doi:10.2514/3.51220

[26] He, L., and Denton, J. D., "Three-Dimensional Time-Marching Inviscid and Viscous Solutions for Unsteady Flows Around Vibrating Blades," *Journal of Turbomachinery*, Vol. 116, No. 3, July 1994, pp. 469–476. doi:10.1115/1.2929436

[27] He, L., "Method of Simulating Unsteady Turbomachinery Flows with Multiple Perturbations," *AIAA Journal*, Vol. 30, No. 11, Nov. 1992, pp. 2730–2735. doi:10.2514/3.11291

C. Tan
Associate Editor